Journal of Hazardous Materials 436 (2022) 129181

Contents lists available at ScienceDirect

Journal of Hazardous Materials

journal homepage: www.elsevier.com/locate/jhazmat

Research Paper

Multi-omics analysis reveals the molecular responses of *Torreya grandis* shoots to nanoplastic pollutant

Chenliang Yu [a,b,1], Hao Zeng [a,b,1], Qi Wang [a,b], Wenchao Chen [a,b], Weijie Chen [a,b], Weiwu Yu [a,b], Heqiang Lou [a,b,*], Jiasheng Wu [a,b,*]

[a] *State Key Laboratory of Subtropical Silviculture, Zhejiang A&F University, Hangzhou, People's Republic of China*
[b] *School of Forestry and Biotechnology, Zhejiang A&F University, Hangzhou, People's Republic of China*

HIGHLIGHTS

- Nanoplastics enhanced the thiobarbituric acid reactive substance content.
- Nanoplastics reduced the concentrations of iron, sulfur, and zinc in *Torreya grandis*.
- Nanoplastics had effect on small RNAs, transcript, proteins, and metabolism levels.
- Nanoplastics can modulate terpenoid and flavonoid biosynthesis pathways.

GRAPHICAL ABSTRACT

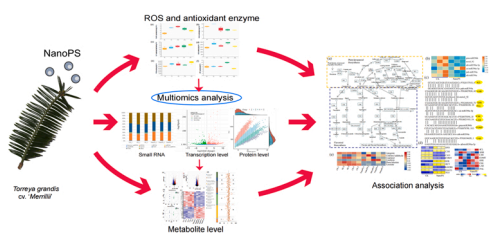

ARTICLE INFO

Editor: Teresa A.P. Rocha-Santos

Keywords:
Flavonoid
Multi-omics
Nanoplastics
Terpenoid
Torreya grandis

ABSTRACT

Micro/nanoplastic has become an emerging pollutant of global concern. At present, ecotoxic researches on micro/nanoplastics mostly focus on marine aquatic organisms and freshwater algae. Research on the ecological impacts of plastics on higher terrestrial plants, especially on forest plants, is relatively limited. *Torreya grandis* cv. Merrillii, a species of conifer in the family Taxaceae, is a unique and economically valuable tree species in China. The physiological and biochemical responses of *T. grandis* seedlings to polystyrene nanoplastics (PSNPs) with a diameter of 100 nm were systematically studied inthe present study. The results showed that nanoplastics enhanced the accumulation of the thiobarbituric acid reactive substance and the activities of catalase and peroxidase. The concentrations of iron, sulfur, and zinc were reduced after nanoplastic exposure. PSNP treatment had an important effect on a series of chemical and genetic indicators of *T. grandis*, includingantioxidants, small RNA, gene transcription, protein expressions, and metabolite accumulation. Multi-omic analysis revealed that PSNPs modulate terpenoid- and flavonoid-biosynthesis pathways by regulating small RNA transcription and protein expression. Our study provided novelty insights into the responses of forest plants to nanoplastic treatment.

1. Introduction

Due to its good engineering characteristics, such as elasticity, portability, plasticity, durability, and low cost, plastic is widely developed and applied in various fields of life and production (Andrady and Neal, 2018). With the increasing demand for plastics, plastic pollution

* Corresponding authors at: State Key Laboratory of Subtropical Silviculture, Zhejiang A&F University, Hangzhou, People's Republic of China.
E-mail addresses: 20170030@zafu.edu.cn (H. Lou), wujs@zafu.edu.cn (J. Wu).
[1] These authors contributed equally to this study.

https://doi.org/10.1016/j.jhazmat.2022.129181
Received 2 April 2022; Received in revised form 12 May 2022; Accepted 16 May 2022
Available online 20 May 2022

has attracted more and more attention from environmentalists (Zhong-Johnson et al., 2021). In 2018, global plastic product production reached 359 million tons and will continue to grow (PlasticsEurope, 2019). Plastic debris has been widely detected in air, ocean, soil, and surface water (Jusko et al., 2016). Plastics in the environment are gradually decomposed into millimeter- (microplastic, 0.1–5 mm) or even nano-scale plastic (nanoplastics, ≤100 nm) fragments under the combined action of mechanical decomposition, biodegradation, photodegradation, and photooxidative degradation (Kurchaba et al., 2020; Radisic et al., 2020). As an emerging pollutant, nanoplastics have attracted extensive attention from scholars because of their small particle size and ability to penetrate cell membranes and even biological barriers. For example, tissue-accumulated nanoplastics can affect the behavior and metabolism of organisms (da Costa et al., 2016; Prüst et al., 2020). Nanoplastics can also become the carriers of exotic species and potential pathogenic microorganisms, causing inestimable potential risks to the entire ecosystem (Gregory, 2009; Prüst et al., 2020). Therefore, nanoplastics are considered extremely dangerous plastic wastes. Micro/nanoplastic is considered a new global pollutant, which exists widely in the atmosphere, water, and soil (Gasperi et al., 2018; Schmidt et al., 2017; Wang et al., 2019). At present, research on micro/nanoplastics mainly comprises environmental investigations focusing on marine, coastal, estuarine, river, and lake ecosystems (Liu et al., 2020; Ruiz-Orejón et al., 2018; Han et al., 2020; Dong et al., 2020). Ecotoxicological research on micro/nanoplastics has focused on aquatic organisms, such as algae, zooplankton, fish, and shellfish (Botterell et al., 2019; Li et al., 2020b; Mak et al., 2019; Rist et al., 2019; Liu et al., 2018, 2022). Nanoplastic-induced growth inhibition or oxidative stress has been frequently described in *Daphnia pulex* , a model organism to study the effect of nanoplastics (Liu et al., 2020; 2021a). Studies of adult zebrafish have shown that microplastics are first ingested and accumulated, resulting in movement changes, intestinal injury, and metabolic changes (Lei et al., 2018; Sleight et al., 2017; Chen et al., 2017). Algae, as lower plants, are often regarded as important environmental receptors, and their adsorption of micro/nanoplastics has been studied extensively. Bhattacharya et al. first discovered that positively charged nanoplastics are physically adsorbed to algae through electrostatic attraction more easily than negatively charged nanoplastics (Bhattacharya et al., 2010). Micro/nanoplastics can reduce photosynthesis in the cell walls and membranes of algae (Nolte et al., 2017; Setälä et al., 2014). Compared with aquatic organisms, the research on the interaction between nanoplastics and terrestrial plants is less, but it also began to increase in recent years. Compared with micro plastics, nanoplastics can indeed enter plant cells. It has been proved that tobacco BY-2 cells absorb polystyrene nanoparticles in cell culture through endocytosis (Bandman et al., 2012). Nanoplastics can inhibit the growth of Arabidopsis, and the degree of inhibition depends on the charge and concentration o nanoparticles. The toxicity of positively charged nanoparticles to Arabidopsis is more significant (Sun et al., 2020). In rice seedlings, fluorescence labeling technology for nanoplastics was used to measure their absorption by plant roots (Zhou et al., 2021). Nanoplastics had no significant effect on the germination rate of wheat seeds, but could affect the root elongation (Lian et al., 2020).

Terrestrial ecosystems have received much less scientific attention regarding micro/nanoplastics than aquatic ecosystems. Plants are the basic components of the ecological environment and play an important role in ecological balance. The transport of industrial nanoparticles can be completed through plant absorption and accumulation (Lecoanet et al., 2004). Microplastics can enter agricultural soil through air deposition, surface runoff, sludge utilization, and agricultural film residue (Gasperi et al., 2018; Schmidt et al., 2017; Wang et al., 2019). Scientific research on the absorption and accumulation of nanoparticles in plants is still in its infancy (Shabbir et al., 2021). *Torreya grandis* belongs to the family Taxaceae (Zhou et al., 2019). *Torreya grandis* contains polyphenols, flavonoids, and many other bioactive substances, which have strong antioxidant activity (He et al., 2016; Shi et al., 2009; Zhang et al., 2022). Studying the effects of nanoplastics on terrestrial plants and their possible toxic mechanisms has practical significance for future assessments of the risk posed by nanoplastics on the terrestrial environment. In this paper, we measured the reactive oxygen species (ROS) level, antioxidant enzyme activity, and element content of *T. grandis* after treatment with nanoplastics, and we analyzed the potential toxic mechanism of nanoplastics for *T. grandis* using multiomic technology. As efficient toxicological research method, integrated transcriptomic, proteomeic and metabolomeic sequencing analysis have been performed to reveal the mechanism of micro/nanoplastic pollutants (Liu et al., 2021a; 2021b; Huang et al., 2021). To better understand the molecular mechanisms by which nanoplastics changed, microRNA sequencing, transcriptome, proteome and metabolome sequencing were used to detect *T. grandis* shoots exposed to nanoplastics, so as to screen the potential genes / proteins / metabolites and signal pathways affected by nanoplastics, and provide potential biomarkers for the risk assessment of forest ecosystem exposed to nanoplastics.

2. Materials and methods

2.1. Plant materials and treatments

One year old *T. grandis* plants were used in this study. Seedlings were treated with polystyrene (about 10 mg / plant). Polystyrene (particle size: ~100 nm; variable coefficient < 3%; sphere) were purchased from Huge Biotechnology (Code: DS010 , Shanghai, China) as a 10% w/v suspension dissolved in sterilized deionized water(contain 0.5% ethanol). Before treatment, the polystyrene was re-dissolved in double distilled water (10 mg/mL) by ultrasonic equipment (KQ500DE, Kunshan Ultrasonic Instruments CO.LTD). Nanoplastics exposed treatments comprising spraying of 10 mg/mL solution to the shoots of *T. grandis* seedlings. Spray with a small pot, 1 mL for each seedling. samples were taken form shoots. After treatment for 7 days, 14 days, 21 days and 28 days, samples were taken form shoots to determine physiological indexes such as antioxidant activity. After each sampling, the samples were frozen in liquid nitrogen and then placed in an 80 °C refrigerator. These enzyme activities were measured simultaneously. After 7 days of treatment, samples were taken to determine microRNA, transcriptome, proteome and metabolome of *T. grandis*.

2.2. Determination of TBARS, H_2O_2, and antioxidant enzyme activities

The activities of catalase (CAT), superoxide dismutase (SOD), peroxidase (POD), and Ascorbic acid peroxidase (APX), along with the contents of thiobarbituric acid reactive substances (TBARSs) and hydrogen peroxide (H_2O_2), were detected using commercially available kits (Suzhou Comin Biotechnology Co. Ltd., China). TBARS content was gained by adopting the thiobarbituric acid method (Ohkawa et al., 1979) (Code: MDA-2-Y, purchase from Suzhou Comin Biotechnology). The H_2O_2 concentration was analyzed according to the method proposed by Islam et al. (2008) (Code: H2O2–2-Y). With H_2O_2 reduction at 405 nm, CAT activity was assessed (Aebi, 1984), and catalytic degradation of 1 μmol H_2O_2 per gram of tissue per minute was defined as an enzyme activity unit (Code: CAT-2-Y). SOD activity was determined by xanthine oxidase (Elstner and Heupel, 1976) (Code: SOD-2-W). When the inhibition rate of the xanthine oxidase coupling reaction system is 50%, the SOD activity in the reaction system is defined as an enzyme activity unit. POD was determined using the guaiacol method (Pick and Keisari, 1980) (Code: POD-2-Y). In the reaction system per milliliter, the change of A470 per gram of tissue per minute is 0.01 as the unit of enzyme activity. APX activity was analyzed by ascorbic acid (AsA) oxidation, whereby 1 nmol AsA is oxidized per minute per gram of tissue as one enzyme activity unit (Code: APX-2-W).

2.3. Determination of element contents

We weighed about 0.1 g of an air-dried and screened sample, put it into a digestion test tube, and added 1 mL of nitric acid. In the DigiBlock digestion system (EH35A, LabTech, UK), the samples were digested at 220 °C. After cooling to room temperature, the digested samples were diluted to 10 mL by ddH_2O and filtered through 0.22-μm filters to determine the content. We determined the elemental content of the diluted samples by employing ICP-MS (Xseries 2 ICP-MS, Thermo,USA). Rubidium(Rb) was used as an internal standard. ICP-MAS calibration standard Kit (code:ICP-MS-CAL2–1,AccuStandard,USA) was used to establish the standard curve and detect he steady state of the instrument. For quality assurance/quality control, the recovery ranges between 80% and 110%.

2.4. RNA isolation and mRNA and sRNA sequencing

The total RNA of the samples was isolated with TRNzol Universal Reagent (DP424, TianGen, Beijing, China) according to the manufacturer's protocol. The purity and concentration of the RNA were measured using a NanoPhotometer® spectrophotometer (IMPLEN, CA, USA) and the Qubit® RNA Assay Kit with a Qubit® 2.0 fluorometer (Life Technologies, CA, USA). The total RNA amount of each 1 or 3 μg sample was used as the input material to construct cDNA or sRNA libraries. cDNA libraries were constructed according to our previous study (Zhan et al., 2021). sRNA libraries were generated by adopting the NEBNext® Multiplex Small RNA Library Prep Set for Illumina® (NEB, USA) following the manufacturer's recommendations, and index codes were added to attribute sequences to each sample. The qualified libraries were sequenced by Illumina Hiseq 2500.

2.5. Read mapping and bioinformatic analysis

Clean reads were obtained by removing reads with adapters, reads containing N (indicating that the base information was unclear), and low-quality reads. The index of the reference genome was constructed by adopting hisat2 v2 0.5, and clear reads were compared with the reference genome. Then, the FPKM of each gene was evaluated by Featurecounts (1.5.0-p3) in terms of the length of the gene, and the reading mapped to the gene was calculated.

The tags of small RNA were mapped to the reference sequence in light of Bowtie without mismatches to evaluate their distribution and expression on the reference. The small RNA tags were mapped to RepeatMasker, the Rfam database, or those types of data from the specified species itself to remove tags originating from protein-coding genes, repeat sequences, rRNA, tRNA, snRNA, and snoRNA. The target gene of miRNA was predicted by psRobot_tar in psRobot. Transcripts per million were adopted to evaluate the expression levels of miRNA according to the following criterion. DESeq R (3.0.3) software was employed for a comparative analysis of the miRNA expression. By default, the threshold for substantially differential expression was set to a corrected P-value of 0.05. For target gene candidates of differentially expressed miRNAs, the Gene Ontology (GO) enrichment distribution was employed. For GO enrichment analysis, a GOseq-based Wallenius non-central hyper-geometric distribution was used to account for gene-length bias. The application KOBAS was used to evaluate the statistical enrichment of the target gene candidates in KEGG pathways.

2.6. Protein extraction and trypsin digestion

A sample of about 0.5 g was completely pestled to final powder in liquid nitrogen. Four times the volume of Tris pH 8.8 buffered phenol extraction buffer (containing 10 mM dithiothreitol, 1% protease inhibitor) was added to each group of samples and ultrasonically lysed. The same volume of Tris was added to the sample and centrifuged for 10 min at 5500×*g* and 4 °C. After centrifugation, we added five times the volume of 0.1 M ammonium acetate/methanol to the supernatant. After overnight precipitation, we washed the precipitation with methanol and acetone successively. The protein concentration of 8 M urea resuspension precipitation was evaluated using the BCA kit.

An equal amount of protein was taken from each sample, and we added 20% TCA, which was mixed by vortex and precipitated for 2 h at 4 °C. The sample was then centrifuged at 4500×*g* for 5 min. The supernatant was discarded and the pellet was washed two or three times with pre-cooled acetone. After drying the precipitate, we added 200 mM tetraethylammonium bromide, ultrasonically dispersed the precipitate, and added trypsin (protease:protein, m/m) at a ratio of 1:50. Then, enzymolysis was conducted overnight. The addition of dithiothreitol changed the concentration to 5 mM, and we reduced it to 56 °C for 30 min and added iodoacetamide. The final concentration was 11 mM and the sample was incubated in the dark at room temperature for 15 min

2.7. TMT labeling, HPLC fractionation, and bioinformatic analysis

Peptides were fractionated by high pH reverse-phase HPLC on an Agilent 300Extend C18 column (5 μm particle size, 4.6 mm id, 250 mm length). The peptide segment gradient was 8–32% acetonitrile with a pH of 9, and 60 components were isolated in 1 h. The peptide segments were then blended into nine components and vacuum freeze-dried. The peptides were separated to use the EASY-nLC 1200 ultra-high performance liquid phase system after being dissolved in phase A of the liquid chromatography mobile phase. Mobile phase A was composed of a 0.1% formic acid and 2% acetonitrile aqueous solution; mobile phase B was composed of a 0.1% formic acid and 90% acetonitrile aqueous solution. The liquid gradient procedure was set at 6–22% B for 0–38 min, 22–32% B for the next 14 min, and then B was increased to 32–80% for 4 min, and 80% B was maintained for the last 4 min. The flow of the mobile phase rate was kept at 500 nL/min. Peptides were separated by UHPLC, injected into the NSI ion source for ionization, and then analyzed using a Q Exactive™ HF-X mass spectrometer. The ion source voltage was set to 2.1 kV, and the peptide precursor ions and their secondary fragments were detected and studied by applying high-resolution Orbitrap. The main mass spectrometer's scanning range was found at 350–1500 *m/z*, with a scanning resolution of 120,000. The data acquisition mode uses the program of data-dependent scanning. That is, after the first-level scan, the precursor ions of the top 20 peptide segments with the highest signal intensity were selected and sequentially joined into the HCD collision cell for fragmentation using 28% of the fragmentation energy mass spectrometry analysis. The automated gain control was adjusted to 3E6, the signal threshold was set to 8.3E4 ions/s, the injection pressure time was tuned to 50 ms, and the dynamic exclusion period of tandem mass spectrometry scanning was fixed to 30 s to avoid excessive repeated sweeps of ions. Fisher's exact test was employed to evaluate the differential expression in the background of the detected proteins, and a P-value of less than 0.05 was considered significant for the GO or KEGG enrichment analysis.

2.8. Metabolite extraction

The plant tissues (80 mg shoots) were snap-frozen by immersion in liquid nitrogen and quickly ground to a powder with a mortar. For metabolite extraction, a 1000 μL methanol/acetonitrile/water (2:2:1, v/v/v) solvent was added to the homogenized samples and centrifuged for 15 min at 14,000×*g* and 4 °C. Then, the supernatant was dried thoroughly in a vacuum centrifuge. For LC-MS analysis, a 100 μL acetonitrile aqueous solution (1:1, v/v) was added to re-dissolve the sample, which was centrifuged for 15 min at 14,000×*g* and 4 °C, and the supernatant was taken and injected for analysis.

2.9. LC-MS/MS analysis

The analysis was performed using an UHPLC (1290 Infinity LC,

Agilent Technologies) coupled to a quadrupole time-of-flight (AB Sciex TripleTOF 6600) from Shanghai Applied Protein Technology Co., Ltd. For HILIC separation, a 2.1 mm × 100 mm ACQUIY UPLC BEH 1.7 μm column (Waters, Ireland) was used to analyze the samples. In the positive and negative modes of ESI, A = water with 25 mM ammonium hydroxide and 25 mM ammonium acetate and B = acetonitrile were selected as the mobile phase. The mobile phase gradient elution procedure was set at 85% B for 1 min, then decreased slowly to 65% over the next 11 min. It was decreased to 40% in 6 s and maintained for 4 min, then increased to 85% in 6 s and re-equilibrated in 5 min

For HPLC separation, the samples were analyzed using a 2.1 mm × 100 mm ACQUIY UPLC HSS T3 1.8 μm column (Waters, Ireland). The column temperature was maintained at 25 °C, the flow rate of gradient elution was maintained at 0.3 mL/min, and the sample infusion volume was 2 μL. In ESI positive mode, the mobile phase composition A = 0.1% formic acid in water and B = 0.1% formic acid in acetonitrile. In ESI negative mode, the mobile phase composition A = water with 0.5 mM ammonium fluoride and B = acetonitrile. The gradient elution procedure was adjusted to 1% B in the first 1.5 min, increased to 99% within 11.5 min, and maintained for 3.5 min. Then, it was decreased to 1% B in 6 s and re-equilibrated in the next 3.4 min

The source setting parameters were set as follows: atomizing gas-assisted heating gas 1 (Gas 1) at 60, auxiliary heating gas 2 (Gas 2) at 60, air curtain gas at 30 psi, ion source temperature at 600 °C, and ion spray voltage floating ± 5500 V (positive and negative modes). In MS-only acquisition, the instrument only collects data in the *m/z* range of 60–1000 Da, and the cumulative time of the TOF MS scan was set to 0.20 s/spectra. In auto-MS/MS acquisition, the instrument accepted an *m/z* range of 25–1000 Da, and the time of production scan was tuned to 0.05 s/spectra. We acquired production scans using Information Dependent Acquisition with high sensitivity mode. Parameter settings: collision energy: 35 V, ± 15 eV; declustering potential: ± 60 V (positive and negative modes); isotopes within 4 Da were precluded and monitored every cycle of candidate ions: 10.

2.10. Bioinformatics of the metabolomic data

The raw data of MS (wiff. scan files) were transformed to MzXML files by employing ProteoWizard MSConvert before being transferred into freely available XCMS software for peak alignment, retention time correction, and peak area extraction. We set the following parameters to pick the peak: centWave *m/z* = 25 ppm, peak width = c (10, 60), prefilter = c (10, 100). We also set the following parameters to group the peak: bw = 5, mzwid = 0.025, and minfrac = 0.5. Isotopes and adducts were annotated through CAMERA (the Collection of Algorithms of MEtabolite pRofile Annotation). Among the extracted ion features, only variables with non-zero measurements greater than 50% in at least one group were retained. Metabolite compounds were identified by comparing the accuracy of *m/z* values (<25 ppm) and MS/MS spectra to an established internal database of available reliable standards. The summed normalized data were analyzed by pareto-scaled principal component analysis (PCA) and orthogonal partial least-squares discriminant analysis (OPLS-DA) using the R package "ropls". The significance of differences between two independent samples was

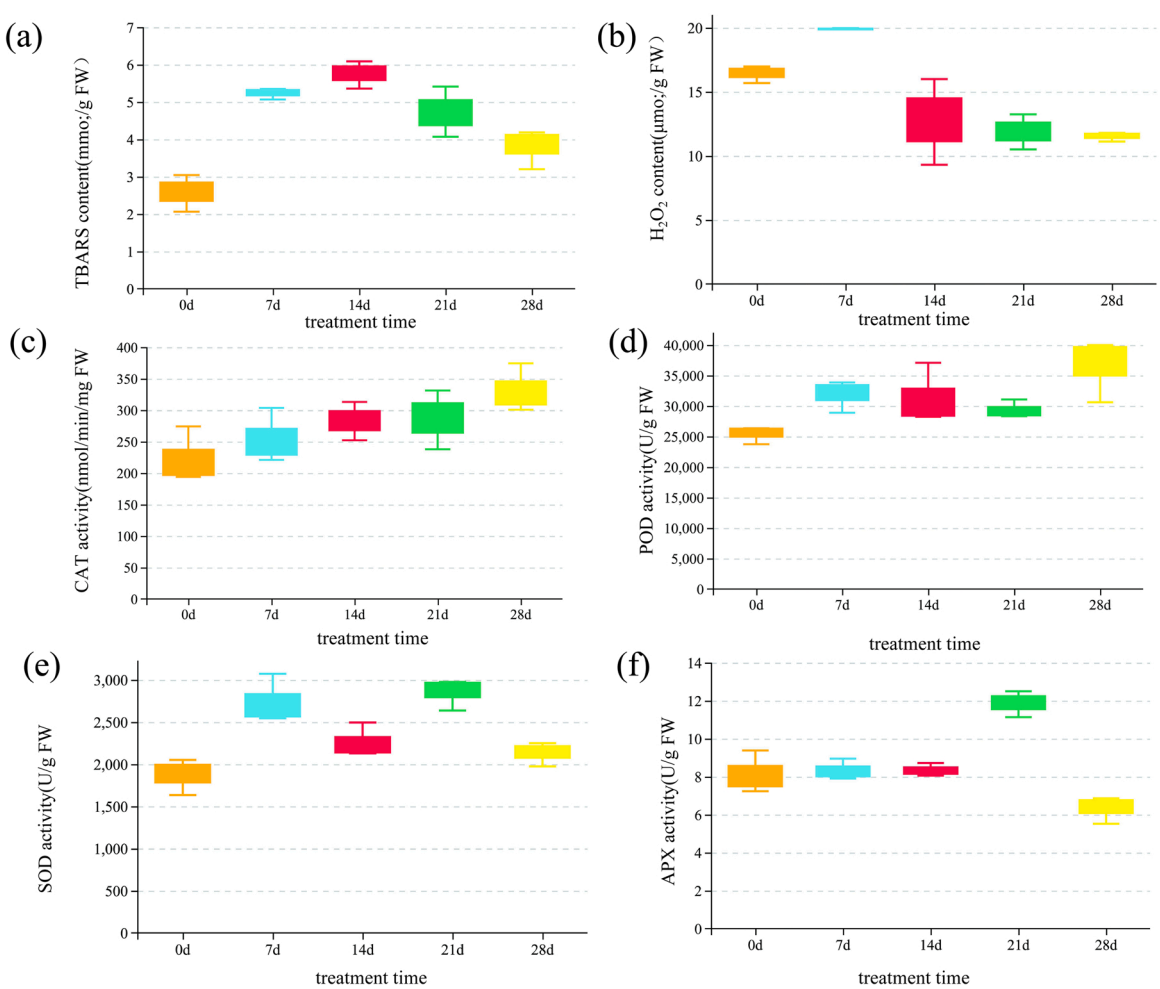

Fig. 1. Oxidative stress responses in *Torreya grandis* shoots mediated by exposure to PSNPs. The content of thiobarbituric acid reactive substances(TBARS)(a) and hydrogen peroxide(H_2O_2)(b). The activity of catalase (CAT)(c), peroxidase (POD) (d), superoxide dismutase (SOD)(e) and ascorbic acid peroxidase (APX) (f).

determined using Student's *t*-test. Variable importance in the projection VIP > 1 and a P-value < 0.05 were used to screen for significantly changed metabolites.

3. Results

3.1. Effects of nanoplastics on the TBARS, H_2O_2, and antioxidant enzyme activities of T. grandis

To assess the effects of nanoplastic stress on *T. grandis* shoots, physiological experiments were performed (Fig. 1). As shown in Fig. 1a, the TBARS content reached the highest level after 14 days of treatment. The H_2O_2 content, reached the highest point after 7 days of treatment, and then declined (Fig. 1b). The activities of CAT and POD increased over the time course of the nanoplastic treatment (Fig. 1c and d). The activities of SOD exhibited dynamic patterns at different time points (Fig. 1e). The activity of APX was relatively stable and high at 21 days (Fig. 1f).

3.2. Overview of T. grandis microRNAomic response to nanoplastic stress

In order to study the effect of nanoplastics on *T. grandis*, microRNAomes were measured. Six libraries of small RNAs were sequenced from *T. grandis* shoots from nanoplastic exposure treatment or control. After filtering, 80,282,135 clean reads were obtained (Table S1). The preponderance of each sample's reads was 21 bp in length (Fig. S1a). The quality of *T.grandis* microRNAome, including, length distribution, pearson correlation, first nucleotide bias and total miRNA nucleotide bias, are additionally shown in Fig. S1. Noncoding RNAs, including rRNA, tRNA, snoRNA, and snRNA were filtered out. There were 284 unique miRNAs in at least one sample group (Table S2). A total of 42 differentially expressed miRNAs, including 19 up- and 23 down-regulated miRNAs, were identified in the nanoplastic treatments,. A heatmap shows differentially miRNA expression patterns under nanoplastic treatment (Fig. 2a). To further analyze the biological functions of *T. grandis* miRNAs, putative targets were predicted for the identified differentially expressed miRNAs using the psRNA Target Server. The putative targets genes of each differentially expressed miRNA are shown in TableS3. We further analyzed the enriched KEGG pathways of the target genes. All predicted target genes were enriched in 116 KEGG pathways (Table S4), and the top 20 enriched pathways are shown in Fig. 2b. The most significantly enriched KEGG pathways are "RNA polymerase" (ko03020), "alpha-Linolenic acid metabolism" (ko00592), "Tryptophan metabolism" (ko00380), "Limonene and pinene degradation" (ko00903), and "Spliceosome" (ko03040) (Fig. 2b and Table S4). The corresponding transcriptome was also determined (Fig. S2). The expression of genes and the GO and KEGG enrichment analyses of differentially expressed genes are shown in Fig. S2 and Tables S5 and S6.

3.3. Impact of nanoplastic treatment on global proteome in T. grandis shoots

We identified the differentially expressed protein response to nanoplastic treatment by applying an integrated approach that involved TMT labeling, HPLC fractionation, and LC-MS/MS analysis. After quality validation, 34,182 peptides were identified (Fig. S3). A total of 6528 proteins were detected, of which 5360 proteins were quantified. Detailed information of all identified proteins, including GO terms, predicted functional domains, KEGG pathways, and subcellular localizations, is listed in Table S7.

A total of 610 differentially expressed protein (DEPs) were identified (Fig. 3 and Table S8). The expression profiles of the DEPs, including 446 up-regulated proteins and 164 down-regulated proteins are shown in a heatmap (Fig. 3a and b). The subcellular location of DEPs was predicted by wolfpsort software (Fig. 3c). Six main subcellular components were identified, including 244 chloroplast-localized DEPs, 153 cytoplasm-localized DEPs, 90 nuclear-localized DEPs, 36 extracellular-localized DEPs, 35 mitochondria-localized DEPs, and 17 plasma membrane-localized DEPs. To predict which physiological processes these differential proteins play a role in, we performed KOG (Fig. 3d), KEGG (Fig. 4a and b), and GO (Fig. 4c and d) analyses. Among the 22 KOG categories, 'Posttranslational modification, protein turnover, chaperones', 'Secondary metabolites biosynthesis, transport and catabolism', and 'Carbohydrate transport and metabolism' contained a large number of unigenes. For the KEGG enrichment analysis, DEPs were assigned to seven pathway terms, such as 'Glutathione metabolism', 'Arachidonic acid metabolism', and 'Photosynthesis-antenna proteins'. For the down-regulated DEPs, 13 significantly enriched KEGG pathways were found, including 'Phenylpropanoid biosynthesis', 'Glycosphingolipid biosynthesis-globo and isoglobo series', and 'Alanine, aspartate and

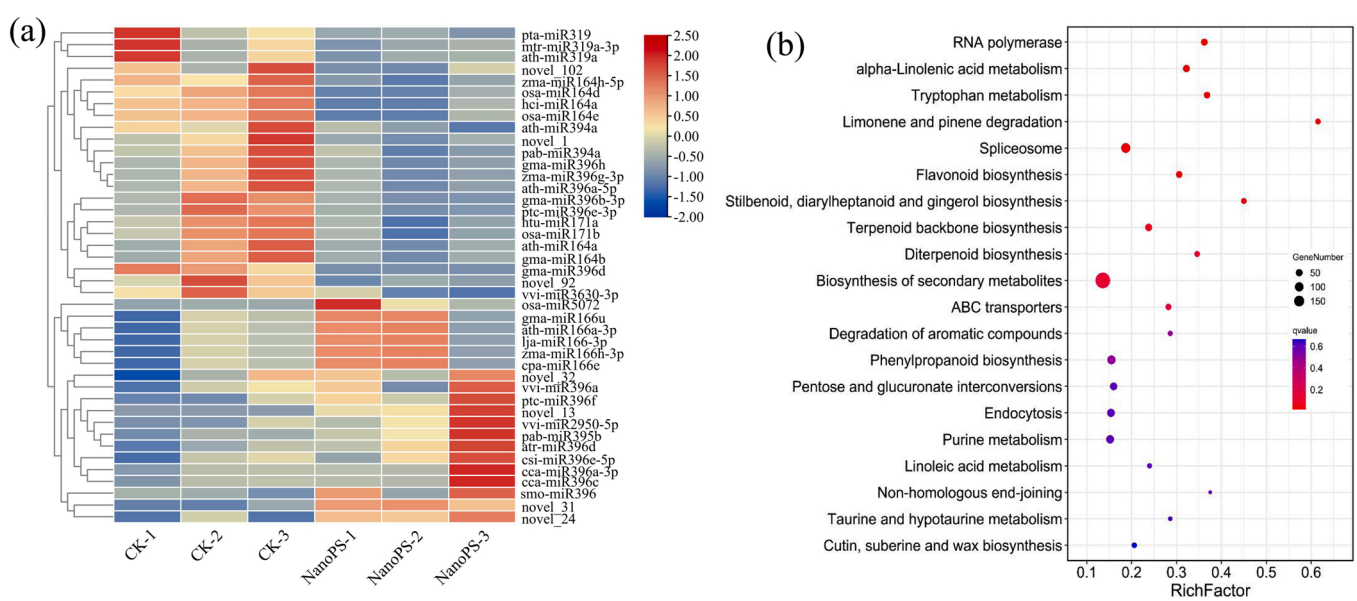

Fig. 2. Overview of PSNPs treatment on *T.grandis* microRNAome. (a) Heat map showing differentially miRNAs expression pattern bwteen different CK and NPs treatments. (b) KEGG enrichment analysis for differentially expressed miRNA predicted target genes. The top 20 enriched KEGG pathways are shown. Circles indicated the gene number in each KEGG pathway. The color bar indicated the range of P value.

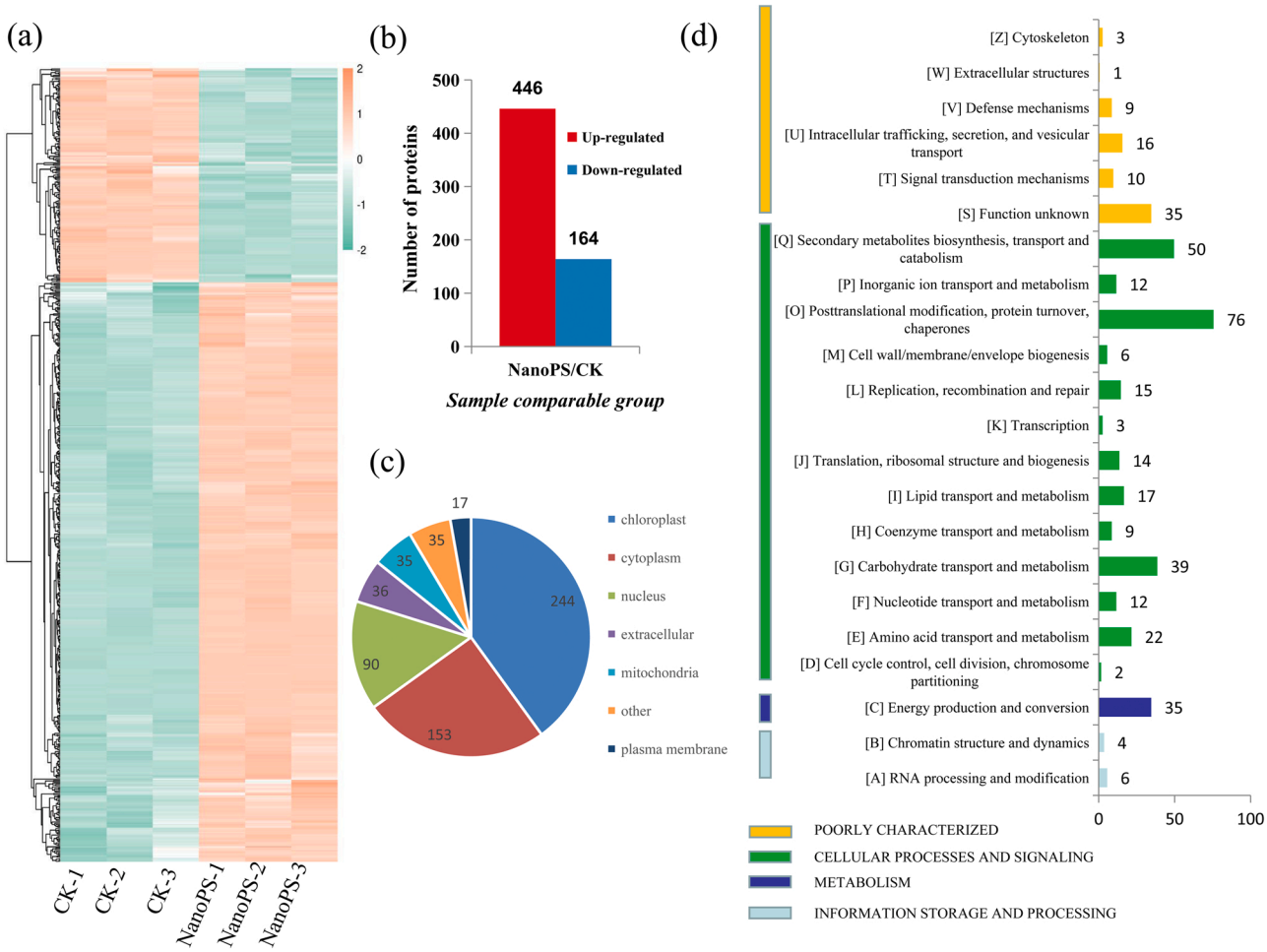

Fig. 3. Impacts PSNPs treatment on proteome levels in *T.grandis*. (a) Expression profiles of the DEPs response to PSNPs treatment. All DEPs were showed in a heatmap. (b) The numbers of up- and down-regulated proteins in the NPs treatment shoots compared to the control. (c) Subcellular distribution of DEPs. (d) KOG functional classification chart of DEPs.

glutamate metabolism'. All DEPs were classified into three categories of different GO terms: 'cellular component', 'molecular function', and. 'biological process'. For the 'Cellular Component' category, the majority of the up-regulated proteins were top-enriched in 'chloroplast thylakoid', 'plastid thylakoid', and 'chloroplast thylakoid membrane'; the down-regulated DEPs were enriched in 'amyloplast', 'apoplast', and 'plant-type cell wall' terms. For the 'Molecular Function' category, the up-regulated DEPs were enriched in 'organic anion transmembrane transporter activity', 'pigment binding', and 'organic acid transmembrane transporter activity' terms, while 'inositol-3-phosphate synthase activity', 'intramolecular lyase activity', and 'adenylosuccinate synthase activity' were the top three enriched terms for the down-regulated DEPs. For the 'Biological Process' category, the up-regulated DEPs were enriched in 'organic anion transport', 'organic acid transport', and 'anion transport', and the down-regulated DEPs were enriched in 'inositol metabolic process', 'polyol biosynthetic process', and 'inositol phosphate metabolic process'. We found that many DEPs were related to the transporter activity and ion tramsmembrane transptort (Fig. 4c and d), so we detected the difference of element content after nanoplastic treatment. Our results indicated that the concentration of iron (Fe), sulfur (S), and zinc (Zn) were reduced after 7 days of nanoplastic exposure. The concentration of potassium (K) and magnesium (Mg) were increased (Fig. 5).

3.4. Effects of nanoplastics on the metabolites in T. grandis leaves

In order to study the effect of nanoplastic treatment on *T. grandis* metabolites, the untargeted metabolomic method was used. PCA showed that the samples were closely gathered in the ESI positive and negative modes, indicating that the repeatability of the experiment was good (Fig. S4). A total of 1873 metabolites were identified in both ESI positive and negative modes (Table S9). By establishing a discriminant model based on OPLS-DA, the differential metabolites related to nanoplastic treatment were selected from the metabolite data set (Fig. 6). The statistical analysis identified 282 differentially accumulated metabolites (DAMs), including 160 up-regulated and 122 down-regulated DAMs based on the following criteria: variable importance in the projection (VIP) > 1.0 and P-value < 0.05 (Fig. 6b and Table S10). An overview of the DAM profiling of the control and nanoplastic treatment *T. grandis* groups is shown in Fig. 6c. These differential metabolites can be classified into 11 categories (Fig. 6d).

3.5. Effect of nanoplastics on terpenoids biosynthesis

The target genes of differential miRNAs were enriched in the terpenoid backbone biosynthesis pathway (Fig. 2b). Some DEPs were enriched in the monoterpenoid biosynthesis and diterpenoidbiosynthesis pathways (Fig. 4a and b). A map of the biochemical pathways related to terpenoid backbone (plastidial 2-C-methyl-D-erythritol phosphate (MEP)and mevalonate (MVA) pathways) in *T. grandis* is

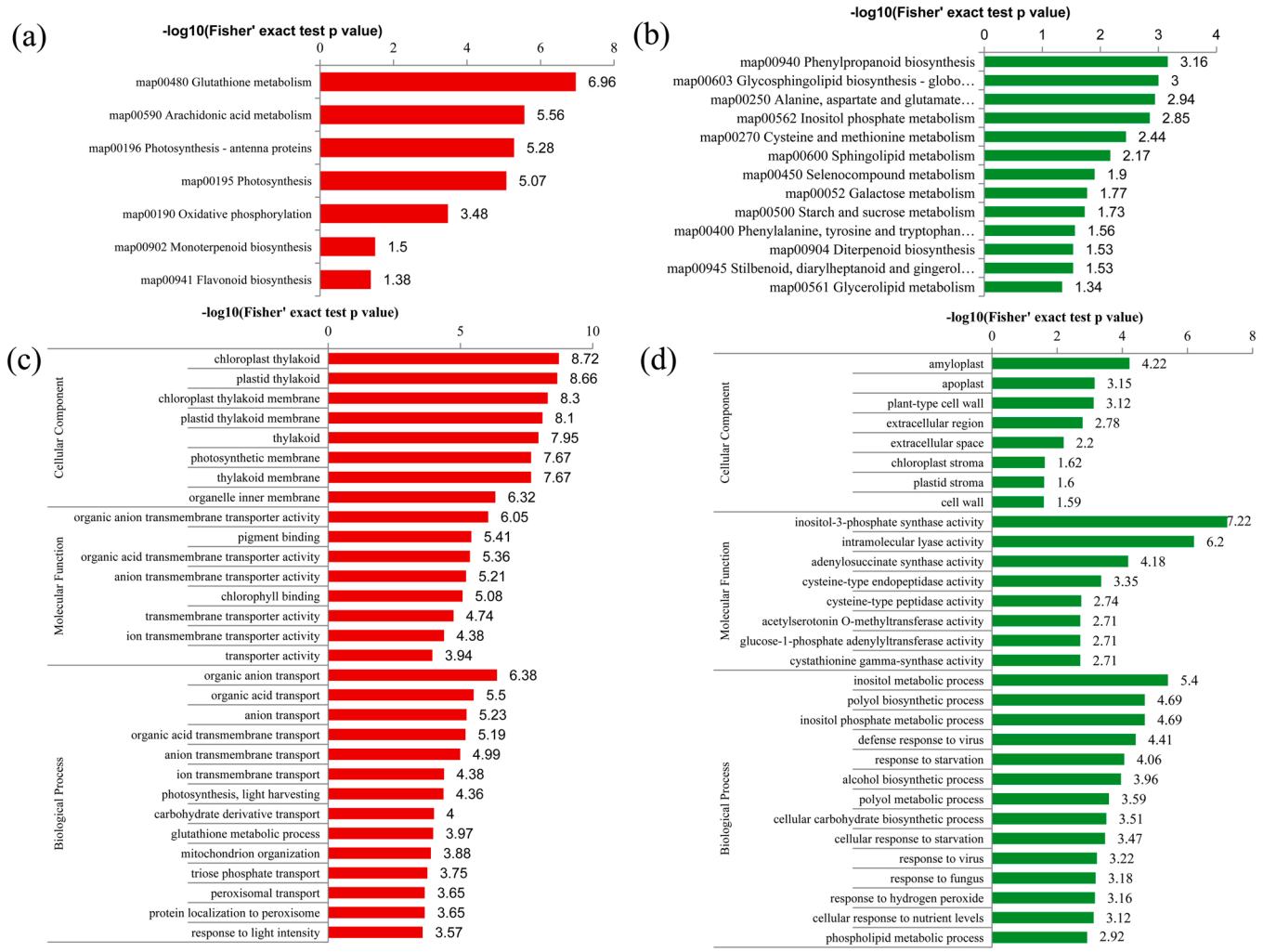

Fig. 4. Enrichment analysis of the DEPs in *T.grandis* after PSNPs treatment. Significantly enriched KEGG terms of the up-regulated (a) and up-regulated (b) proteins. Distribution of the up-regulated (c) and down-regulated (d) proteins with GO enrichment analysis.

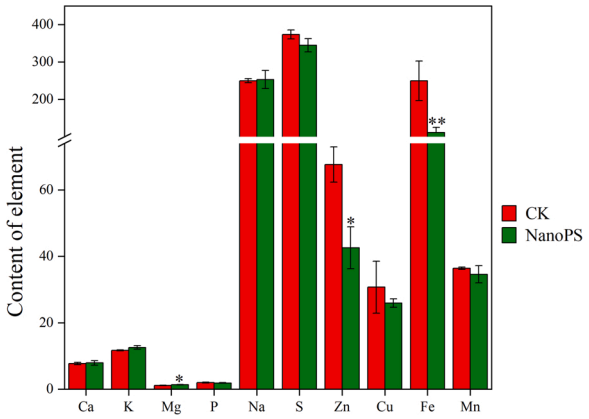

Fig. 5. Effect of PSNPs treatment on element contents in *T.grandis*. "*" represents $P < 0.05$ and "**" represents $P < 0.01$, using unpaired student *T*-test. The concentration of potassium, calcium, magnesium and phosphorus is mg/g dry weight. Other element concentrations are μg/g dry weight.

shown in Fig. 7a. The predicted targets of differentially expressed miRNAs included three key terpenoid backbone biosynthesis genes: 4-Hydroxy-3-methylbut-2-enyl diphosphate reductase (HDR), 3-Hydroxy-3-methylglutaryl-CoA reductase (HMGR), and geranylgeranyl pyrophosphate synthase (GGPPS) (Fig. 7b and c). Four unigenes were annotated as HMGR in the *T. grandis* transcriptome (Fig. 7d). These genes were the potential targets of osa-miR164e and zma-miR164h-5p (Fig. 7c). HDR was a potential target ofpab-miR394a, and GGPPS was a potential target of ath-miR164a. The expression of GGPPS was down-regulated at the transcriptional and protein levels (Fig. 7d). The intermediate metabolites of the terpenoid backbone, monoterpenoid, and diterpenoidbiosynthesis were further analyzed. The contents of three differential metabolites (mevalonic acid, loganic acid, and abietic acid) increased in the nanoplastic treatment group. The other three differential metabolites (carvone, gibberellic acid, and bisdemethoxycurcumin) decreased in the nanoplastic treatment group (Fig. 7e).

3.6. *Effect of nanoplastics on phenylpropanoid and flavonoid biosynthesis*

Our results indicated that the target genes of differential miRNAs were enriched in the phenylpropanoid and flavonoid biosynthesis pathways (Fig. 2b). Moreover, DEPs were enriched in the flavonoid biosynthesis pathway (Fig. 4a and b). Therefore, we further analyzed the effect of nanoplastics on the biosynthesis of phenylpropanoids and flavonoids. A map of the biochemical pathways related to phenylpropanoid and flavonoid biosynthesis in *T. grandis* is shown in Fig. 8a. A total of six differentially expressed miRNAs were identified, most of which decreased in the nanoplastic treatment group, except csi-miR396e-5p (Fig. 8b). The target genes of these miRNAs contained eight key genes:

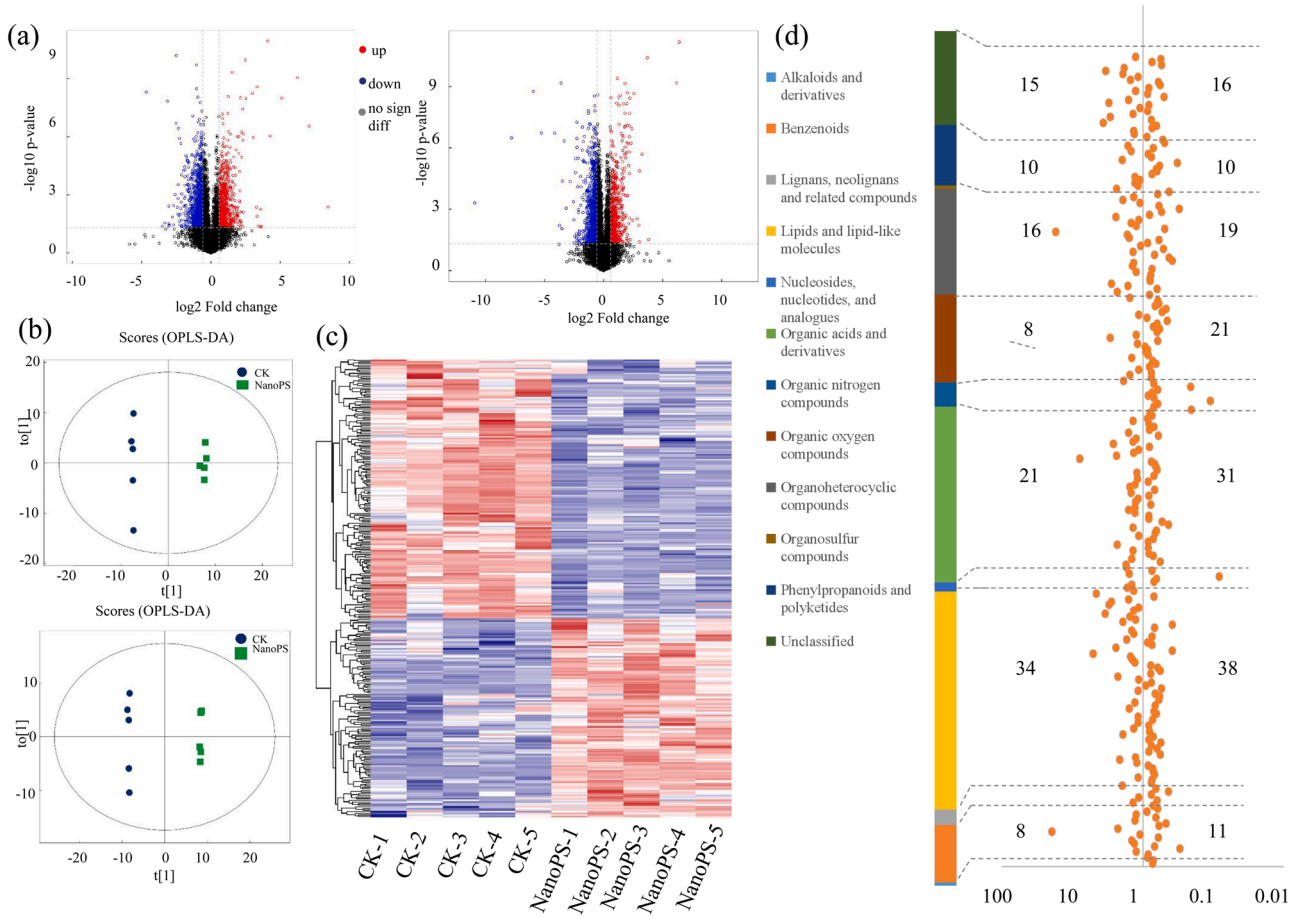

Fig. 6. Impacts PSNPs treatment on metabolite levels in *T.grandis*. (a) Volcanic map of differential metabolites in both ESI+ and ESI− modes. Based on univariate analysis, the differences of all metabolites (including unidentified metabolites) detected in positive and negative ion modes were analyzed. The differential metabolites with FC > 1.5 or FC < 0.67 and P value < 0.05 are visually displayed in the form of volcanic map. Black represents metabolites having no significant differences, red represents upregulated metabolites, blue represents downregulated metabolites.(b) The OPLS-DA score plot shows groupings of control and PSNPs treated samples in both ESI+ and ESI− modes. t[1] represents principal component 1, to [1] represents principal component 2, and ellipse represents 95% confidence interval. The dots of the same color represent the biological repeats within the group, and the distribution state of the dots reflects the degree of difference between and within the group. (c) Heat map of control and PSNPs treated samples varieties at the metabolome level. The relative quantitative values of differentiated metabolites were transformed into Z values and clustered. Different color regions represent different clustering information. The metabolic expression patterns within the same group are similar, which indicates that they may have similar functions or participate in the same biological process. (d) Classification of differential metabolites. The relative abundances of the metabolites belonging to various major metabolic categories.

PAL: *phenylalanine ammonia lyase*, *4CL*: *4-coumarate: CoA ligase*, *F3H*: *flavanone 3-hydroxylase*, *ANR*: *anthocyanidin reductase*, *COMT*: *caffeic acid 3-O-methyltransferase*, *LAR*: *leucoanthocyanidin reductase*, *DFR*: *dihydroflavonolreductase*, and *C4H*: *Cinnamic acid 4-hydroxylase* (Fig. 8c). The transcriptional expression of 4CL, DFR, F3H, and LAR were up-regulated by nanoplastic treatment (Fig. 8d). And some key enzymes, including anthocyanidin synthase, DFR, shikimate O-hydroxycinnamoyltransferase, and flavonol synthase, were up-regulated by nanoplastic treatment at the protein level (Fig. 8d). Based on the KEGG enrichment analysis results of differential metabolites, six differential metabolites were identified as intermediates in the phenylpropanoid and flavonoid biosynthesis pathways. Among them, the content of Coniferyl aldehyde and Coniferin were increased in the nanoplastic treatment group (Fig. 8e).

4. Discussion

Recently, the public has become aware of the ubiquity of micro/nanoplastics in fresh water systems and the ocean, and of the serious environmental challenges they pose. Compared with aquatic ecosystems, there are relatively few studies on micro/nanoplastic pollution in terrestrial ecosystems, especially agricultural ecosystems (Piehl et al., 2018). It is estimated that with the extensive use of plastic films and agricultural chemicals containing microplastics, the accumulation of microplastics in agricultural soil is more than that in marine environment (de Souza Machado et al., 2019). Higher plants play an important role in the balance of terrestrial ecosystems, but research on the ecotoxicological effects of micro/nanoplastics on plants, particular in trees, is still in its infancy (Bosker et al., 2019). In this paper, the responses of small RNA, transcripts, proteins, and metabolites of *T. grandis* to the exposure of polystyrene nanoplastics exposure were studied by multi-omics. Our study provides a scientific basis for the study of ecological toxicity and ecological risk of nanoplastics to forests.

Previous studies on the toxic effects of micro/nanoplastics on plants and their toxic mechanism have focused on lower aquatic plants (algae). Many studies have reported that micro/nanoplastics can reduce the growth of algae and cause oxidative stress damages (Li et al., 2020a; Wu et al., 2019; Zhang et al., 2017). The inhibition effect of microplastics on algae photosynthesis and growth increases with a decrease in plastic particle size (Sjollema et al., 2016). It was found that nanoplastics hinder the absorption and utilization of light energy and CO_2 by microalgae and affect photosynthesis by adsorbing on the surface of *Duchenna teteri*, so as to inhibit the growth of microalgae (Bergami et al., 2017). The antioxidant system of the microalgae itself cannot remove

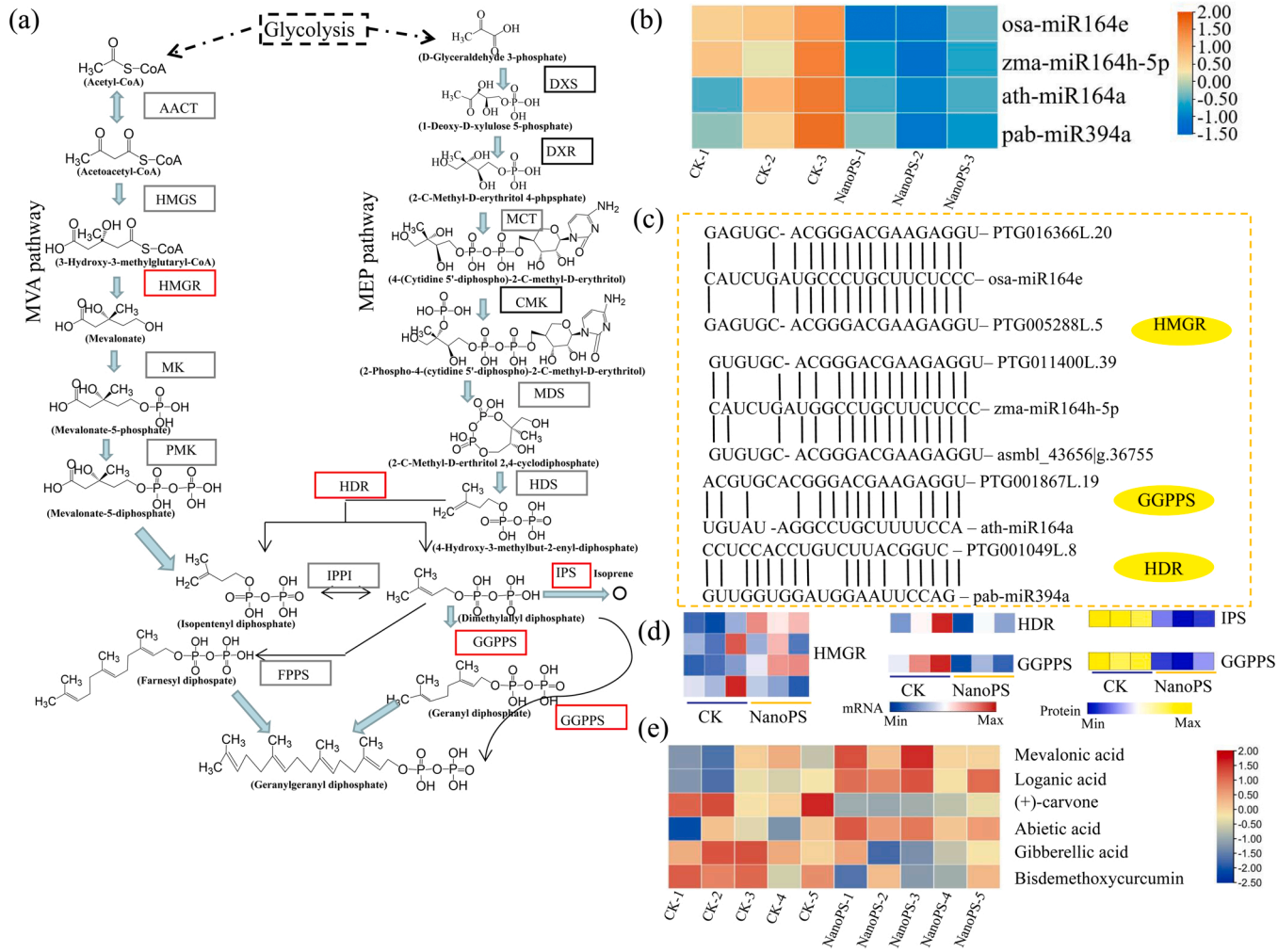

Fig. 7. Visualization of sRNA, transcript, protein and metabolite expression related to terpenoid backbone biosynthesis in *Torreya grandis*. (a) Overview of the Overview of the MVA and MEP pathways in *Torreya grandis*. The red box indicates the identified differential gene/protein. (b) Expression changes of four differentially expressed miRNAs identified in terpenoid backbone biosynthesis. (c) Target genes were identified for the four differentially expressed miRNAs. Enzyme abbreviations: HDR:4-Hydroxy-3-methylbut-2-enyl diphosphate reductase. HMGR: 3-Hydroxy-3-methylglutaryl-CoA reductase. GGPPS: geranylgeranyl pyrophosphate synthase. (d) Expression changes of the differentially expressed miRNAs target genes were at protein and transcript level.(e) Accumulation of differentiated metabolites associated with terpenoid backbone, monoterpenoid and Diterpenoid biosynthesis under PSNPs treatment in *T.grandis*. Z-score fold change values are shown on a color scale that is proportional to the abundance of each miRNA, unigene and metabolite.

excess ROS that was induced by nanoplastic in cells, resulting in oxidative damage to cells and oxidative stress response (Bhattacharya et al., 2010). KEGG enrichment analysis showed that the target genes of differential microRNAs, differential genes, and differential proteins were enriched into the photosynthesis pathway, indicating that nanoplastics may affect the photosynthesis of *T. grandis* leaves, which is consistent with the effects of nanoplastics on algae. SOD and POD activities in fava bean plants increased significantly after exposure to 5 μM/100 nm PS MPS (10–100 mg/L). The difference of enzyme activity in plants after exposure to PSNPs may depend on plastic particle size, dose level, and plant species (Jiang et al., 2019). The results of this study show that nanoplastics can induce the accumulation of TBARS and the increase of antioxidant enzyme activities, such as CAT and POD after treatment. It is speculated that nanoplastics have oxidative toxicity to *T. grandis*.

As a carrier of environmental metal elements, micro/nanoplastics increase their migration ability in the environment and the corresponding environmental risks (Naik et al., 2019; Yu et al., 2019). Pb, chromium, and Zn have obvious adsorption on microplastics on polyethylene and polyvinyl chloride, and Al, Fe, Cu, Pb, and Zn adsorption levels can be as high as 300 pg/g (Godoy et al., 2019; Holmes et al., 2012). In addition, the biofilms formed on the surface of microplastics promote their adsorption of metals (Richard et al., 2019). On the other hand, nanoplastics affect the absorption of nutrient elements in animal and plant, which may be due to the influence of ion transporter activity (Lian et al., 2020; Li et al., 2022). In this study, many differential proteins were enriched in “anion transporter activity”, “transporter activity”, “ion transporter activity”, “transporter activity”, “anion transport”, “anion transmembrane transport”, and “ion transmembrane transport” GO terms. The absorption and transport of nutrient elements (Fe, S, and Zn) by *T. grandis* were partially hindered, and the results were similar in wheat (Lian et al., 2020). Studies in wheat have shown that the absorption and transport of metal elements are selectively inhibited, because nanoplastics can differentially regulate the expression of genes related to metal ion transport (Lian et al., 2020).

So far, little is known about the molecular mechanism of nanoplastic-mediated phytotoxicity in plants. However, transcriptome and proteomic analyses provide information and knowledge about nanoplastic-induced toxicity in higher plant because they can provide a link between gene/protein up-regulation and down-regulation (Ruotolo et al., 2018; Landa et al., 2017). Omic methods have successfully identified some reactions, which point to several potential toxic pathways and the

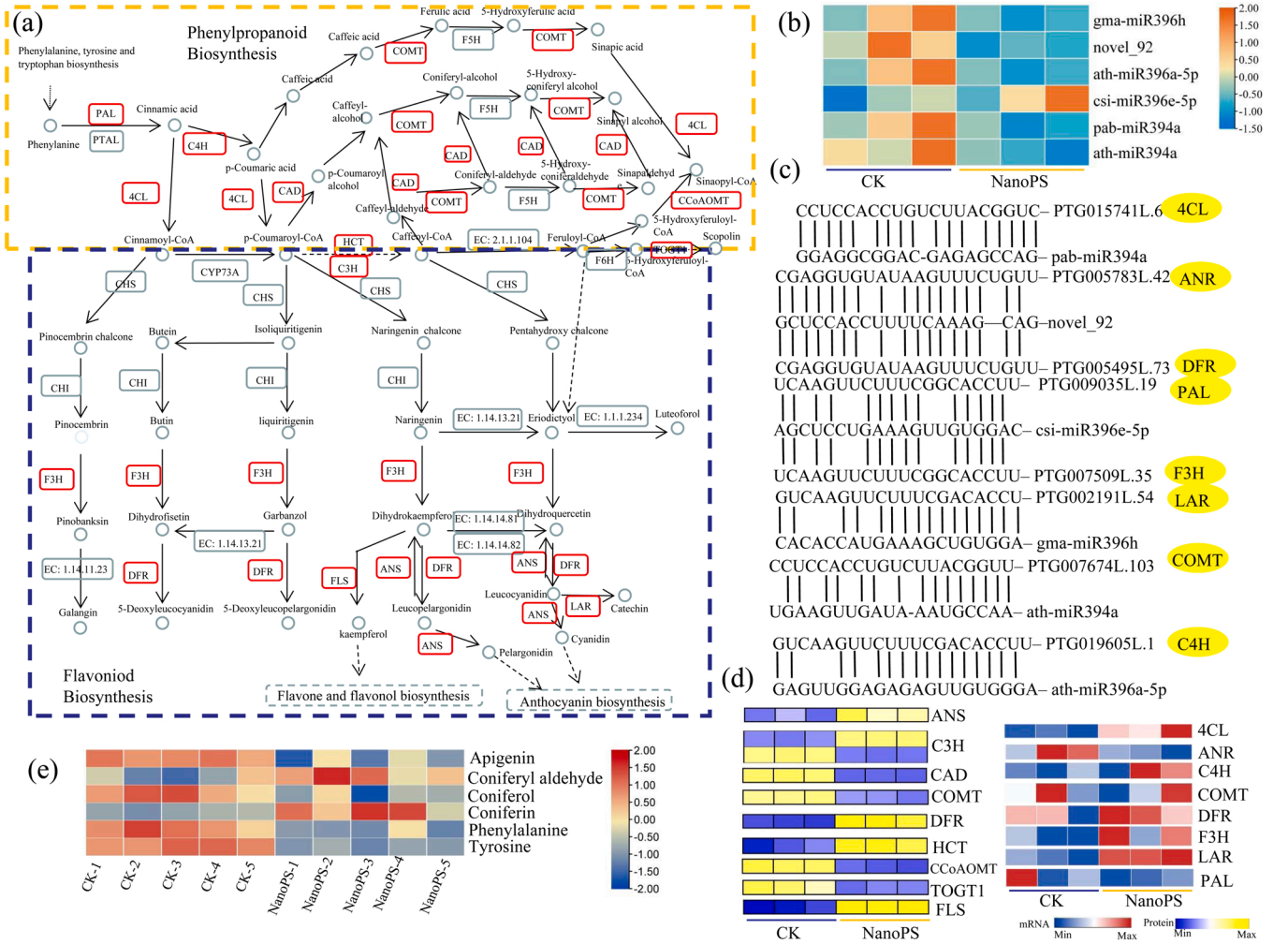

Fig. 8. Visualization of sRNA, transcript, protein and metabolite expression in a biochemical pathway map related to flavonoid biosynthesis in *T.grandis*. (a) Overview of the phenylpropanoid- and flavonoid-related biosynthesis pathway in *T.grandis*. The red box indicates the identified differential gene / protein. (b) Expression changes of Six differentially expressed miRNAs identified in phenylpropanoid- and flavonoid-related biosynthesis pathway.(c) Target genes were identified for the six differentially expressed miRNAs. Enzyme abbreviations: PAL: phenylalanine ammonia lyase, 4CL: 4-coumarate:CoA ligase, F3H: flavanone 3-hydroxylase, ANR: anthocyanidin reductase. COMT: Caffeoyl-CoA O-methyltransferase. LAR:leucoanthocyanidin reductase. DFR: dihydroflavonolreductase. (d) Expression changes of the differentially expressed miRNAs target genes were at protein and transcript level. (e) Accumulation of differentiated metabolites associated with phenylpropanoid flavonoid biosynthesis under PSNPs treatment in *T.grandis*. Z-score fold change values are shown on a color scale that is proportional to the abundance of each miRNA, unigene and metabolite.

action modes of nanoplastics. The secondary metabolites of the phenylpropanoid and terpenoid pathways were shown to act as a pivotal part in the stress response of plants (Pandey et al., 2017; Pateraki and Kanellis, 2010). Terpenoids are natural products that exist widely in nature, including monoterpenes, sesquiterpenes, diterpenes, and polyterpenes, such as kinetin, gibberellin, carotenoids, sterols, chlorophyll, etc (Bohlmann and Keeling, 2008; Zhang et al., 2015). Plant secondary metabolite terpenoids play an important role in stress and biological interaction (Ormeno and Fernandez, 2012). HMGR is the rate-limiting enzyme of terpene biosynthesis in eukaryotes (Friesen and Rodwell, 2004). GGPPS, which synthesizes common precursor geranyl pyrophosphate required for chlorophyll, carotenoids, and volatile olefins, is the most critical step among the many steps in the terpenoid biosynthesis pathway (Gao et al., 2018). In our study, the expression levels of miRNAs that targeted *HMGR* and *GGPPS* h were changed significantly under nanoplastic treatment. It is suggested that nanoplastics take part in the activation of the *T. grandis* terpenoid biosynthesis pathway by regulating miRNAs such as osa-miR164e, zma-miR164h-5p, and ath-miR164a. Phenylpropanoid pathway provides the precursors of lignin, flavonoids, and other secondary metabolites (Tohge and Fernie, 2017). These biomolecules are essential for managing the structure of the cell wall in response to a range of stressors. Studies have shown that industrial nanomaterials can cause the overexpression of phenylpropanoid metabolism and other stress response-related genes. This indicates that the increase of fibrosis or lignification of the cell wall in plants makes it more difficult to absorb nutrients and water, and then reduces plant biomass and chlorophyll content (Nair and Chung, 2014). Flavonoids (including anthocyanins) are considered to play a major antioxidant role in the responses of plants to a variety of abiotic stresses (Brunetti et al., 2013). In our study, the expression levels of miRNAs that targeted *4CL*, *ANS*, *COMT*, *C4H*, *DFR*, *F3H*, *LAR*, and *PAL* were changed significantly under nanoplastic treatment. The expression of *4CL*, *C4H*, *DFR*, *F3H*, and *LAR* at the transcriptional level was up-regulated by nanoplastic treatment. Our results show that nanoplastics play a role in activating the biosynthetic pathway of phenylpropane and flavonoids in *T. grandis* by regulating miRNAs. In *D.pulex*, nanoplastics induce the accumulation of reactive oxygen species and affect the MAPK-HIF-1/NFkB-mediated antioxidant system (Liu et al., 2020). These results show that the detoxification mechanism of terrestrial plants to nanoplastics is different from that of aquatic organism.

5. Conclusions

In conclusion, this study showed that PSNP treatment had an important effect on a series of chemical and genetic indicators of *T. grandis* shoots, including antioxidants, small RNA and gene transcription, protein expression, and metabolite accumulation. Nanoplastics enhanced the TBARS content and the activities of CAT and POD. Small RNA and transcriptome and proteome analyses suggested that nanoplastics may affect photosynthesis in *T. grandis* shoots. The Fe, S, and Zn were reduced after nanoplastic exposure. A large number of metabolites were identified by untargeted metabolomics. Multiomic analysis revealed that PSNPs can modulate terpenoid and flavonoid biosynthesis pathways by modulating small RNA expression and protein levels. Our study provided novelty insights into the responses of forest plants to nanoplastic treatment.

CRediT authorship contribution statement

Chenliang Yu: Conceptualization, Methodology, Resources, Formal analysis, Investigation, Data curation, Visualization, Writing – original draft, Writing – review & editing. **Hao Zeng:** Conceptualization, Resources, Visualization, Data curation, Writing – review & editing. **Wenchao Chen:** Conceptualization, Methodology, Resources. **Weijie Chen:** Data curation, Writing – review & editing. **Weiwu Yu:** Conceptualization, Methodology, Funding acquisition. **Heqiang Lou:** Conceptualization, Methodology, Visualization, Supervision, Writing – review & editing, Project administration, Funding acquisition. **Jiasheng Wu:** Conceptualization, Methodology, Resources, Visualization, Supervision, Writing – review & editing, Project administration, Funding acquisition.

Declaration of Competing Interest

The authors declare that they have no known competing financial interests or personal relationships that could have appeared to influence the work reported in this paper.

Acknowledgments

We thank International Science Editing (http://www.internationalscienceediting.com) for editing this manuscript. This work was supported by the Breeding of New Varieties of *Torreya grandis Program* (2021C02066-11); Scientific R&D Foundation for Talent Start-up Project of Zhejiang A&F University (2020FR073 and 2018FR028); the National Natural Science Foundation of China (Grant no. 32171830). The funders had no role in study design, data collection and analysis, decision to publish, or preparation of the manuscript.

Environmental Implication

With increasing worldwide plastic production and consumption, plastic wastes have become a global concern. Micro/nanoplastic are widely distributed in various environmental media, including bottled and natural waters, air, sediments, and soils. Research on the ecological impact of plastics on higher terrestrial plants is relatively limited, especially toxicity research on forest plants. *Torreya grandis* is an important and precious nut in China. We analyzed the potential toxic mechanism of nanoplastics for *T. grandis* using multiomic technology. Our study provides new insights into the effects of nanoplastic on the growth of forest plants.

Appendix A. Supporting information

Supplementary data associated with this article can be found in the online version at doi:10.1016/j.jhazmat.2022.129181.

References

Aebi, H., 1984. Catalase in Vitro, Methods in Enzymology. Academic Press, pp. 121–126.
Andrady, A.L., Neal, M.A., 2018. Applications and societal benefits of plastics. Philos. Trans. R. Soc. Lond. B Biol. Sci. 364, 1977–1984.
Bandmann, V., Müller, J.D., Köhler, T., Homann, U., 2012. Uptake of fluorescent nano beads into BY2-cells involves clathrin-dependent and clathrin-independent endocytosis. FEBS Lett. 586, 3626–3632.
Bergami, E., Pugnalini, S., Vannuccini, M.L., Manfra, L., Faleri, C., Savorelli, F., Dawson, K.A., Corsi, I., 2017. Long-term toxicity of surface-charged polystyrene nanoplastics to marine planktonic species Dunaliella tertiolecta and Artemia franciscana. Aquat. Toxicol. 189, 159–169.
Bhattacharya, P., Lin, S., Turner, J.P., Ke, P.C., 2010. Physical adsorption of charged plastic nanoparticles affects algal photosynthesis. J. Phys. Chem. C 114, 16556–16561.
Bohlmann, J., Keeling, C.I., 2008. Terpenoid biomaterials. Plant J. 54, 656–669.
Bosker, T., Bouwman, L.J., Brun, N.R., Behrens, P., Vijver, M.G., 2019. Microplastics accumulate on pores in seed capsule and delay germination and root growth of the terrestrial vascular plant Lepidium sativum. Chemosphere 226, 774–781.
Botterell, Z.L.R., Beaumont, N., Dorrington, T., Steinke, M., Thompson, R.C., Lindeque, P. K., 2019. Bioavailability and effects of microplastics on marine zooplankton: a review. Environ. Pollut. 245, 98–110.
Brunetti, C., Di Ferdinando, M., Fini, A., Pollastri, S., Tattini, M., 2013. Flavonoids as antioxidants and developmental regulators: relative significance in plants and humans. Int. J. Mol. Sci. 14, 3540–3555.
Chen, Q., Gundlach, M., Yang, S., Jiang, J., Velki, M., Yin, D., Hollert, H., 2017. Quantitative investigation of the mechanisms of microplastics and nanoplastics toward zebrafish larvae locomotor activity. Sci. Total Environ. 584–585, 1022–1031.
da Costa, J.P., Santos, P.S.M., Duarte, A.C., Rocha-Santos, T., 2016. Nano)plastics in the environment – Sources, fates and effects. Sci. Total Environ. 566–567, 15–26.
de Souza Machado, A.A., Lau, C.W., Kloas, W., Bergmann, J., Bachelier, J.B., Faltin, E., Becker, R., Görlich, A.S., Rillig, M.C., 2019. Microplastics can change soil properties and affect plant performance. Environ. Sci. Technol. 53, 6044–6052.
Dong, M., Luo, Z., Jiang, Q., Xing, X., Zhang, Q., Sun, Y., 2020. The rapid increases in microplastics in urban lake sediments. Sci. Rep. 10, 848.
Elstner, E.F., Heupel, A., 1976. Inhibition of nitrite formation from hydroxylammoniumchloride: a simple assay for superoxide dismutase. Anal. Biochem. 70, 616–620.
Friesen, J.A., Rodwell, V.W., 2004. The 3-hydroxy-3-methylglutaryl coenzyme-A (HMG-CoA) reductases. Genome Biol. 5, 248.
Gao, Y., Wei, W., Zhao, X., Tan, X., Fan, Z., Zhang, Y., Jing, Y., Meng, L., Zhu, B., Zhu, H., Chen, J., Jiang, C.-Z., Grierson, D., Luo, Y., Fu, D.-Q., 2018. A NAC transcription factor, NOR-like1, is a new positive regulator of tomato fruit ripening. Hortic. Res. 5, 75.
Gasperi, J., Wright, S.L., Dris, R., Collard, F., Mandin, C., Guerrouache, M., Langlois, V., Kelly, F.J., Tassin, B., 2018. Microplastics in air: are we breathing it in? Curr. Opin. Environ. Sci. Health. 1, 1–5.
Godoy, V., Blázquez, G., Calero, M., Quesada, L., Martín-Lara, M.A., 2019. The potential of microplastics as carriers of metals. Environ. Pollut. 25, 113363.
Gregory, M.R., 2009. Environmental implications of plastic debris in marine settings-entanglement, ingestion, smothering, hangers-on, hitch-hiking and alien invasions. Phil. Trans. R. Soc. B 364, 2013–2025.
Han, M., Niu, X., Tang, M., Zhang, B.-T., Wang, G., Yue, W., Kong, X., Zhu, J., 2020. Distribution of microplastics in surface water of the lower Yellow River near estuary. Sci. Total Environ. 707, 135601.
He, Z., Zhu, H., Li, W., Zeng, M., Wu, S., Chen, S., Qin, F., Chen, J., 2016. Chemical components of cold pressed kernel oils from different *Torreya grandis* cultivars. Food Chem. 209, 196–202.
Holmes, L.A., Turner, A., Thompson, R.C., 2012. Adsorption of trace metals to plastic resin pellets in the marine environment. Environ. Pollut. 160, 42–48.
Huang, W., Wang, X., Chen, D., Xu, E.G., Luo, X., Zeng, J., Huan, T., Li, L., Wang, Y., 2021. Toxicity mechanisms of polystyrene microplastics in marine mussels revealed by high-coverage quantitative metabolomics using chemical isotope labeling liquid chromatography mass spectrometry. J. Hazard. Mater. 417, 126003.
Islam, E., Liu, D., Li, T., Yang, X., Jin, X., Mahmood, Q., Tian, S., Li, J., 2008. Effect of Pb toxicity on leaf growth, physiology and ultrastructure in the two ecotypes of Elsholtzia argyi. J. Hazard. Mater. 154, 914–926.
Jiang, X., Chen, H., Liao, Y., Ye, Z., Li, M., Klobučar, G., 2019. Ecotoxicity and genotoxicity of polystyrene microplastics on higher plant Vicia faba. Environ. Pollut. 250, 831–838.
Jusko, T.A., Oktapodas, M., Palkovičová Murinová, L., Babinská, K., Babjaková, J., Verner, M.A., DeWitt, J.C., Thevenet-Morrison, K., Čonka, K., Drobná, B., Chovancová, J., Thurston, S.W., Lawrence, B.P., Dozier, A.M., Järvinen, K.M., Patayová, H., Trnovec, T., Legler, J., Hertz-Picciotto, I., Lamoree, M.H., 2016. Demographic, reproductive, and dietary determinants of perfluorooctane sulfonic (PFOS) and perfluorooctanoic acid (PFOA) concentrations in human colostrum. Environ. Sci. Technol. 50, 7152–7162.
Kurchaba, N., Cassone, B.J., Northam, C., Ardelli, B.F., LeMoine, C.M.R., 2020. Effects of MP polyethylene microparticles on microbiome and inflammatory response of larval zebrafish. Toxics 8, 55.
Landa, P., Dytrych, P., Prerostova, S., Petrova, S., Vankova, R., Vanek, T., 2017. Transcriptomic response of *Arabidopsis thaliana* exposed to CuO nanoparticles, bulk material, and ionic copper. Environ. Sci. Technol. 51, 10814–10824.
Lecoanet, H.F., Bottero, J.Y., Wiesner, M.R., 2004. Laboratory assessment of the mobility of nanomaterials in porous media. Environ. Sci. Technol. 38, 5164–5169.

Lei, L., Wu, S., Lu, S., Liu, M., Song, Y., Fu, Z., Shi, H., Raley-Susman, K.M., He, D., 2018. Microplastic particles cause intestinal damage and other adverse effects in zebrafish *Danio rerio* and nematode *Caenorhabditis elegans*. Sci. Total Environ. 619–620, 1–8.
Li, S., Wang, P., Zhang, C., Zhou, X., Yin, Z., Hu, T., Hu, D., Liu, C., Zhu, L., 2020a. Influence of polystyrene microplastics on the growth, photosynthetic efficiency and aggregation of freshwater microalgae *Chlamydomonas reinhardtii*. Sci. Total Environ. 714, 136767.
Li, Y., Liu, Z., Li, M., Jiang, Q., Wu, D., Huang, Y., Jiao, Y., Zhang, M., Zhao, Y., 2020b. Effects of nanoplastics on antioxidant and immune enzyme activities and related gene expression in juvenile *Macrobrachium nipponense*. J. Hazard Mater. 398, 122990.
Li, Y., Liu, Z., Jiang, Q., Ye, Y., Zhao, Y., 2022. Effects of nanoplastic on cell apoptosis and ion regulation in the gills of *Macrobrachium nipponense*. Environ Pollut 300, 118989.
Lian, J., Wu, J., Xiong, H., Zeb, A., Yang, T., Su, X., Su, L., Liu, W., 2020. Impact of polystyrene nanoplastics (PSNPs) on seed germination and seedling growth of wheat (Triticum aestivum L.). J. Hazard. Mater. 385, 121620.
Liu, Z., Cai, M., Yu, P., Chen, M., Wu, D., Zhang, M., Zhao, Y., 2018. Age-dependent survival, stress defense, and AMPK in Daphnia pulex after short-term exposure to a polystyrene nanoplastic. Aquat. Toxicol. 204, 1–8.
Liu, Z., Huang, Y., Jiao, Y., Chen, Q., Wu, D., Yu, P., Li, Y., Cai, M., Zhao, Y., 2020. Polystyrene nanoplastic induces ROS production and affects the MAPK-HIF-1/NFkB-mediated antioxidant system in *Daphnia pulex*. Aquat. Toxicol. 220, 105420.
Liu, Z., Li, Y., Pérez, E., Jiang, Q., Chen, Q., Jiao, Y., Huang, Y., Yang, Y., Zhao, Y., 2021a. Polystyrene nanoplastic induces oxidative stress, immune defense, and glycometabolism change in Daphnia pulex: Application of transcriptome profiling in risk assessment of nanoplastics. J. Hazard. Mater. 402, 123778.
Liu, Z., Li, Y., Sepúlveda, M., Jiang, Q., Jiao, Y., Chen, Q., Huang, Y., Tian, J., Zhao, Y., 2021b. Development of an adverse outcome pathway for nanoplastic toxicity in *Daphnia pulex* using proteomics. Sci. Total Environ. 766, 144249.
Liu, Z., Malinowski, C., Sepulveda, M., 2022. Emerging trends in nanoparticle toxicity and the significance of using Daphnia as a model organism. Chemosphere 291, 132941.
Mak, C.W., Yeung, K.C.-F., Chan, K.M., 2019. Acute toxic effects of polyethylene microplastic on adult zebrafish. Ecotoxicol. Environ. Saf. 182, 109442.
Naik, R.K., Naik, M.M., D'Costa, P.M., Shaikh, F., 2019. Microplastics in ballast water as an emerging source and vector for harmful chemicals, antibiotics, metals, bacterial pathogens and HAB species: A potential risk to the marine environment and human health. Mar. Pollut. Bull. 149, 110525.
Nair, P.M., Chung, I.M., 2014. A mechanistic study on the toxic effect of copper oxide nanoparticles in Soybean (*Glycine max* L.) root development and lignification of root cells. Biol. Trace Elem. Res. 162, 342–352.
Nolte, T.M., Hartmann, N.B., Kleijn, J.M., Garnæs, J., van de Meent, D., Jan Hendriks, A., Baun, A., 2017. The toxicity of plastic nanoparticles to green algae as influenced by surface modification, medium hardness and cellular adsorption. Aquat. Toxicol. 183, 11–20.
Ohkawa, H., Ohishi, N., Yagi, K., 1979. Assay for lipid peroxides in animal tissues by thiobarbituric acid reaction. Anal. Biochem. 95, 351–358.
Ormeno, E., Fernandez, C., 2012. Effect of soil nutrient on production and diversity of volatile terpenoids from plants. Curr. Bioact. Compds. 8, 71–79.
Pandey, S.P., Srivastava, S., Goel, R., Lakhwani, D., Singh, P., Asif, M.H., Sane, A.P., 2017. Simulated herbivory in chickpea causes rapid changes in defense pathways and hormonal transcription networks of JA/ethylene/GA/auxin within minutes of wounding. Sci. Rep. 7, 44729.
Pateraki, I., Kanellis, A.K., 2010. Stress and developmental responses of terpenoid biosynthetic genes in *Cistus creticus* subsp. *creticus*. Plant Cell Rep. 29, 629–641.
Pick, E., Keisari, Y., 1980. A simple colorimetric method for the measurement of hydrogen peroxide produced by cells in culture. J. Immunol. Methods 38, 161–170.
Piehl, S., Leibner, A., Löder, M.G.J., Dris, R., Bogner, C., Laforsch, C., 2018. Identification and quantification of macro- and microplastics on an agricultural farmland. Sci. Rep. 8, 17950.
PlasticsEurope, 2019. The Facts 2019: an Analysis of European Plastics Production.
Prüst, M., Meijer, J., Westerink, R.H.S., 2020. The plastic brain: neurotoxicity of micro- and nanoplastics. Part. Fibre Toxicol. 17, 24.
Radisic, V., Nimje, P.S., Bienfait, A.M., Marathe, N.P., 2020. Marine plastics from Norwegian West Coast Carry potentially virulent fish pathogens and opportunistic human pathogens harboring new variants of antibiotic resistance genes. Microorganisms 8, 1200.
Richard, H., Carpenter, E.J., Komada, T., Palmer, P.T., Rochman, C.M., 2019. Biofilm facilitates metal accumulation onto microplastics in estuarine waters. Sci. Total Environ. 683, 600–608.
Rist, S., Baun, A., Almeda, R., Hartmann, N.B., 2019. Ingestion and effects of micro- and nanoplastics in blue mussel (*Mytilus edulis*) larvae. Mar. Pollut. Bull. 140, 423–430.
Ruiz-Orejón, L.F., Sardá, R., Ramis-Pujol, J., 2018. Now, you see me: high concentrations of floating plastic debris in the coastal waters of the Balearic Islands (Spain). Mar. Pollut. Bull. 133, 636–646.
Ruotolo, R., Maestri, E., Pagano, L., Marmiroli, M., White, J.C., Marmiroli, N., 2018. Plant response to metal-containing engineered nanomaterials: an omics-based perspective. Environ. Sci. Technol. 52, 2451–2467.
Schmidt, C., Krauth, T., Wagner, S., 2017. Export of plastic debris by rivers into the Sea. Environ. Sci. Technol. 51, 12246–12253.
Setälä, O., Fleming-Lehtinen, V., Lehtiniemi, M., 2014. Ingestion and transfer of microplastics in the planktonic food web. Environ. Pollut. 185, 77–83.
Shabbir, S., Kulyar, M.Fe.A., Bhutta, Z.A., Boruah, P., Asif, M., 2021. Toxicological consequences of titanium dioxide nanoparticles (TiO2NPs) and their jeopardy to human population. BioNanoSci 11, 621–632.
Shi, H., Wang, H., Wang, M., Li, X., 2009. Antioxidant activity and chemical composition of *Torreya grandis* cv. Merrillii seed. Nat. Prod. Commun. 4, 1565–1570.
Sjollema, S.B., Redondo-Hasselerharm, P., Leslie, H.A., Kraak, M.H.S., Vethaak, A.D., 2016. Do plastic particles affect microalgal photosynthesis and growth? Aquat. Toxicol. 170, 259–261.
Sleight, V.A., Bakir, A., Thompson, R.C., Henry, T.B., 2017. Assessment of microplastic-sorbed contaminant bioavailability through analysis of biomarker gene expression in larval zebrafish. Mar. Pollut. Bull. 116, 291–297.
Sun, X., Yuan, X., Jia, Y., Feng, L., Zhu, F., Dong, S., Liu, J., Kong, X., Tian, H., Duan, J., Ding, Z., Wang, S., Xing, B., 2020. Differentially charged nanoplastics demonstrate distinct accumulation in Arabidopsis thaliana. Nat. Nanotechnol. 15, 755–760.
Tohge, T., Fernie, R.A., 2017. An overview of compounds derived from the shikimate and phenylpropanoid pathways and their medicinal importance. Mini Rev. Med. Chem. 17, 1013–1027.
Wang, J., Liu, X., Li, Y., Powell, T., Wang, X., Wang, G., Zhang, P., 2019. Microplastics as contaminants in the soil environment: a mini-review. Sci. Total Environ. 691, 848–857.
Wu, Y., Guo, P., Zhang, X., Zhang, Y., Xie, S., Deng, J., 2019. Effect of microplastics exposure on the photosynthesis system of freshwater algae. J. Hazard. Mater. 374, 219–227.
Yu, F., Yang, C., Zhu, Z., Bai, X., Ma, J., 2019. Adsorption behavior of organic pollutants and metals on micro/nanoplastics in the aquatic environment. Sci. Total Environ. 694, 133643.
Zhan, Y., Wu, T., Zhao, X., Wang, Z., Chen, Y., 2021. Comparative physiological and full-length transcriptome analyses reveal the molecular mechanism of melatonin-mediated salt tolerance in okra (*Abelmoschus esculentus* L.). BMC Plant Biol. 21, 180.
Zhang, C., Chen, X., Wang, J., Tan, L., 2017. Toxic effects of microplastic on marine microalgae *Skeletonema costatum*: Interactions between microplastic and algae. Environ. Pollut. 220, 1282–1288.
Zhang, F., Ma, Z., Qiao, Y., Wang, Z., Chen, W., Zheng, S., Yu, C., Song, L., Lou, H., Wu, J., 2022. Transcriptome sequencing and metabolomics analyses provide insights into the flavonoid biosynthesis in Torreya grandis kernels. Food Chem. 374, 131558.
Zhang, X., Allan, A., Li, C., Wang, Y., Yao, Q., 2015. *De Novo* assembly and characterization of the transcriptome of the Chinese medicinal herb, *Gentiana rigescens*. Int. J. Mol. Sci. 16, 11550–11573.
Zhong-Johnson, E., Voigt, C.A., Sinskey, A.J., 2021. An absorbance method for analysis of enzymatic degradation kinetics of poly(ethylene terephthalate) films. Sci. Rep. 11, 928.
Zhou, C.-Q., Lu, C.-H., Mai, L., Bao, L.-J., Liu, L.-Y., Zeng, E.Y., 2021. Response of rice (*Oryza sativa* L.) roots to nanoplastic treatment at seedling stage. J. Hazard. Mater. 401, 123412.
Zhou, X., Shang, J., Qin, M., Wang, J., Jiang, B., Yang, H., Zhang, Y., 2019. Fractionated antioxidant and anti-inflammatory kernel oil from *Torreya fargesii*. Molecules 24, 3402.